Resistivity anisotropy of tilted columnar W and W–Cu thin films

Raya El Beainou, Jean-Marc Cote, Vincent Tissot, Valérie Potin, Nicolas Martin

▶ **To cite this version:**

Raya El Beainou, Jean-Marc Cote, Vincent Tissot, Valérie Potin, Nicolas Martin. Resistivity anisotropy of tilted columnar W and W–Cu thin films. Surface and Coatings Technology, 2021, 421, pp.127412 (11). 10.1016/j.surfcoat.2021.127412 . hal-03359918

HAL Id: hal-03359918
https://hal.science/hal-03359918

Submitted on 2 Aug 2023

HAL is a multi-disciplinary open access archive for the deposit and dissemination of scientific research documents, whether they are published or not. The documents may come from teaching and research institutions in France or abroad, or from public or private research centers.

L'archive ouverte pluridisciplinaire **HAL**, est destinée au dépôt et à la diffusion de documents scientifiques de niveau recherche, publiés ou non, émanant des établissements d'enseignement et de recherche français ou étrangers, des laboratoires publics ou privés.

Distributed under a Creative Commons Attribution - NonCommercial 4.0 International License

Version of Record: https://www.sciencedirect.com/science/article/pii/S0257897221005867
Manuscript_1b45950a38da6a26292c8713d02789b2

Resistivity anisotropy of tilted columnar W and W-Cu thin films

Raya El Beainou[1], Jean-Marc Cote[1], Vincent Tissot[1], Valérie Potin[2], Nicolas Martin[1, *]

* Author to whom correspondence should be addressed: nicolas.martin@femto-st.fr.

© 2021 published by Elsevier. This manuscript is made available under the CC BY NC user license
https://creativecommons.org/licenses/by-nc/4.0/

[1] *Institut FEMTO-ST, UMR 6174, CNRS, ENSMM, Univ. Bourgogne Franche-Comté, 15B, Avenue des Montboucons, 25030 BESANCON Cedex, France*

[2] *Laboratoire Interdisciplinaire Carnot de Bourgogne (ICB), UMR 6303, CNRS, Univ. Bourgogne Franche-Comté, 9, Avenue Alain Savary, BP 47 870, F-21078 DIJON Cedex, France*

Abstract:

Electrical resistivity of tilted columnar thin films is theoretically and experimentally investigated considering the anisotropic structure of the columns. To this end, W and W-Cu thin films were deposited by the GLAD co-sputtering technique. These films were prepared using two different sputtering pressures: 2.5×10^{-3} and 15×10^{-3} mbar. Their morphological and crystallographic properties were studied in order to understand the correlations between some structural characteristics and electrical behaviors of these structured films. The influence of the sputtering pressure on the film's morphology was demonstrated and related to the electronic transport properties in these columnar films. For W-Cu films, the copper was chemically etched in order to tune even more the electrical properties. By rotating the sample along its azimuthal axis, it was shown that the measured resistivity in the axis perpendicular to the particle flux is maximum, but decreases significantly along the axis parallel to the flux, leading to an anisotropic resistivity coefficient higher than 1.9 for some films. Similarly, an analytical model based-on effective medium approximations was successfully applied to determine the evolution of electrical resistivity versus azimuthal axis for W, W-Cu and etched W-Cu thin films.

Keywords: sputtering pressure; GLAD; W films; W-Cu films; electrical resistivity.

1. Introduction

Thin films produced by physical vapor deposition processes are of particular interest in the field of materials and surfaces. Since properties of thin films are directly related to their structure, strategies to modify their structure at the micro- and nano-scale have always been a major topic. Nanofabrication techniques attempt to control thermal [1], mechanical [2], electrical [3-5], acoustic [6-8], optical [9] and magnetic [10] properties, and can create new effects. Among these nanofabrication techniques, an original approach has been developed since the end of the 90s, called GLAD (GLancing Angle Deposition) [11]. The latter proposes a new bottom-up method for structuring vacuum-deposited thin films. This method consists in developing a coating under oblique incidence on a fixed or mobile substrate. By controlling the growth direction of the films, it then becomes possible to give them some particular architectures: tilted columns, zigzags, helices and so on [12]. The GLAD technique is characterized by only two key parameters that can influence the growth mechanism of thin films, i.e., the incidence angle of the particle flux impinging on the growing film, and the rotation of the substrate during the deposition stage. Their variation leads to a wide range of physical properties. By adjusting these two operating parameters as well as the structuring of the substrate surface and/or the type of material, the GLAD technique has become a real toolbox capable of producing a wide range of architectures. Since the majority of GLAD films have porous nanostructures and interesting behaviors, they appear to be ideal candidates for several applications [13]. In addition to the design of new and novel structures, these GLAD thin films also present novel and extended properties compared to conventional systems [14, 15].

Among physical and chemical properties of GLAD thin films, the electrical conductivity can be particularly tuned and connected to the film's architecture. For metal compounds, electrical conductivity is closely related to the behavior of electrons. Several mechanisms must be

considered in order to understand the electronic transport phenomena in thin films. Thus, the electrical properties of metals become even more complex for thin films with certain anisotropic structures such as an oriented columnar architecture [16]. For this purpose, different theoretical models have been developed to predict the electrical properties of metallic films. These models are based on the evolution of the conductivity of metals as a function of their microstructure, in particular the correlation with the grain size and thickness of films [17–19]. In addition, a few researches have been performed about changes in conductivity due to a controlled orientation of the columnar structure in thin films [20]. The effect of this orientation is even more verified for theoretical models that take into account these special architectures and can calculate the transport properties in such anisotropic materials [21]. Ueda *et al.* [16] studied the conductivity in Fe/Si multilayered films manufactured by GLAD and found that the anisotropy of the conductivity increased with the incidence angle of particles and the films porosity. Several authors reported on correlations between electrical properties and porosity of GLAD films [3-5, 7, 8]. However, accurate porosity measurements of GLAD thin films still remain an open challenge which become even more complex for the GLAD co-sputtering process. Similar results were found by Zhong *et al.* [22] in indium tin oxide nanorods manufactured by GLAD. Vick and Brett [23] used Monte Carlo simulations to model the growth of the nanostructures and then predicted the conductivity of Ti chevrons manufactured by OAD based on the simulated structure and a random walk model of electron transport. Besnard *et al*. [24] proposed an analytical model based on the grain boundary conductivity model of Pichard *et al*. [25]., and successfully applied to chromium thin films On the other hand, percolation theory has also been used to understand and model isotropic and anisotropic transport phenomena in composite and disordered media [26]. Precise analytical expressions of percolation transport for specific geometries have been obtained using efficient medium approximations (EMAs). EMAs are

average field theories that replace random individual conductance between neighboring sites with an effective conductance that describes the macroscopic transport of the system [5, 26]. Song *et al*. [5] have studied the electrical properties of the metallic thin film consisting of tilted Ag nanorod arrays fabricated by OAD. They implemented the AB^2-EMA model to describe the conductivity of such arrays and provided insight into their structural properties.

In this paper, we study the influence of the sputtering pressure used during the GLAD process on the electrical behaviors of the W and W-Cu tilted columnar structures produced by sputtering and co-sputtering. The motivation is to understand experimentally and theoretically relationships between the structural and electronic transport properties of these films. To that end, a theoretical model is developed to better understand the phenomena influencing the electron transport in these media. The role of the geometry and size of the architectures is particularly investigated considering the anisotropic character of the deposited films. Thus, three types of films are prepared: pure W films, W-Cu films and chemically etched W-Cu films (copper is etched to get a more porous structure). In addition, the electrical resistivity of W and W-Cu films before and after copper etching is measured as a function of the azimuthal angle in order to study the resistivity anisotropy in such columnar structures. The theoretical model is used to verify the influence of column geometry on the electrical resistivity of the films.

2. Experimental details

W-Cu and W thin films were deposited by DC magnetron sputtering in a 40 L homemade vacuum chamber at a base pressure below 10^{-8} mbar. Tungsten and copper metallic targets with a purity of 99.9 at % and a diameter of 51 mm, were used. The current of the tungsten target was fixed at I_W = 140 mA and that of the copper target at I_{Cu} = 50 mA for W-Cu films, and I_{Cu}= 0 mA for W films. Glass and (100) silicon substrates were fixed at the center of the

substrate holder which was inclined at an angle of 80° (i.e., W and Cu targets were inclined at the same angle $\alpha_W = \alpha_{Cu} = 80°$). The latter was at $d_{W\text{-}S} = 65$ mm from the tungsten target and at $d_{Cu\text{-}S} = 95$ mm from the copper target. The deposition time was adjusted to get a film thickness close to 1000 nm. This order of magnitude frees from the dependence of the film's thickness on electrical properties. It is indeed commonly reported that resistivity *vs.* thickness of polycrystalline films saturates for thicknesses higher than about 100 nm due to scattering on grain boundaries. For GLAD films and due to the rising of the porous structure as a function of the thickness, we fixed the same value (1000 nm) for all films so as to neglect the films' thickness dependency and to compare them to each other's. The wet chemical etching of W-Cu thin films was carried out in a ferric chloride $FeCl_3$ solution at room temperature for an etching time of 1 min 30 s. Samples were then immersed in deionized water to stop the wet chemical etching process and remove the residue of ferric chloride. More details about the experimental setup can be found in previous works [8, 27, 28].

The morphology (surface and cross-section views) of W and W-Cu thin films was observed by scanning electron microscopy (SEM) in a Dual Beam SEM/FIB FEI Helios 600i microscope. W and W-Cu thin films were produced at two different argon sputtering pressures. Targets were sputtered with Ar flow rates of 1.6 sccm and 12 sccm at a pumping speed of 13 Ls^{-1}. The resulting Ar sputtering pressures were $p = 2.5\times10^{-3}$ mbar and 15×10^{-3} mbar, respectively. Crystal structure of the films was characterized by X-ray diffraction (XRD). Measurements were carried out using a Bruker D8 focus diffractometer with a Cobalt X-ray tube (Co $\lambda K\alpha_1 = 0.178897$ nm) with a $\theta/2\theta$ configuration. Scans were performed with a step of 0.02° per 0.2s and a 2θ angle ranging from 20 to 80°. Such a configuration only probes crystallographic planes parallel to the sample surface. Finer and deeper analyses about the crystal structure, especially anisotropic crystal size and orientation would certainly be suitable, especially for GLAD films since out-of-plane orientation, as well as in-plane

alignment is of prime influence on the films' properties [29, 30]. However, such a study about the crystallographic orientation of grains in tilted columnar thin films requires further investigations, which are out of the scope of the paper.

The electrical resistivity was measured as a function of the azimuthal angle by the four-probe van der Pauw configuration [31]. Bierwagen *et al.* [32] proposed an original procedure to obtain anisotropic transport properties, especially from the results of the van der Pauw measurements. They developed an original procedure to determine the components of the resistivity tensor. Such approach allows getting in-plane conductivity σ_{xx} (Sm^{-1}) and σ_{yy} (Sm^{-1}) (and thus, the corresponding resistivity ρ_{xx} (Ωm) and ρ_{yy} (Ωm)) in the mutually perpendicular directions x, y of the two-dimensional plane, respectively. The anisotropic coefficient A is then deduced from the resistivity ratio. To this aim, electrical resistivity measurements of films deposited on glass substrate were performed in air at room temperature. The measurement area was a 10x10 mm^2 square. In order to characterize the orientation-dependent resistivity, the W, W-Cu and W-Cu etched films were rotated from an azimuthal angle $\varphi = 0°$ to 180° (Fig. 1) followed by 4-point measurements. After each rotation step of 20-25°, the electrical resistivity anisotropy was determined.

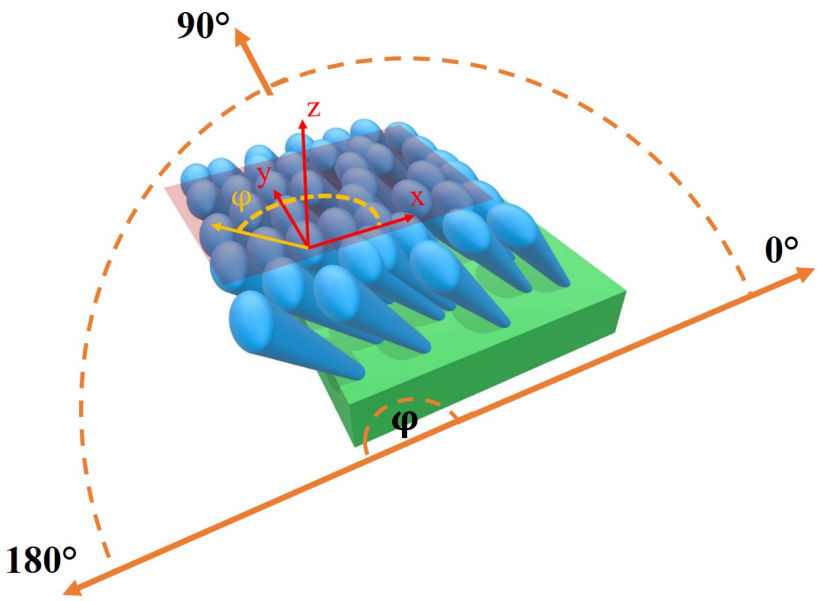

Figure 1: Schematic representation illustrating the film orientation used for resistivity measurements as a function of the azimuthal angle φ.

The Tencor Alpha Step IQ profilometer was used to measure the thickness of deposited films. Heterogeneity of thickness was obtained using the GLAD technique. In order to have an accurate thickness measurement, several measurements were performed on the same sample but at different locations. These measurements were performed in the center of the sample (i.e., ± 5 mm from the center). Then e_m represents the average value of about ten thickness measurements performed over a distance of 1 cm close to the center of the sample.

3. Theory

Song *et al.* [5] proposed that the percolation model [26] of a disordered resistance network can be applied to the morphology of the columnar structure. The AB^2-EMA method of Bernasconi [33] is an application of the effective medium theory in anisotropic media. This method has been used to calculate the resistivity of W, W-Cu films before and after Cu etching. Indeed, the effective medium used in the percolation model consists in replacing the

random resistance network by an invariant medium in which the conductance G_i of the links simulates the electrical properties of the random medium.

It is assumed that the conductance, namely G_i, describes the transport of charges along the individual column and that the latter is connected to the neighboring column with the probability p_i that a charge (an electron in our case) passes from one column to another, where i = ⊥ or // to the particle fluxes (Fig. 2)

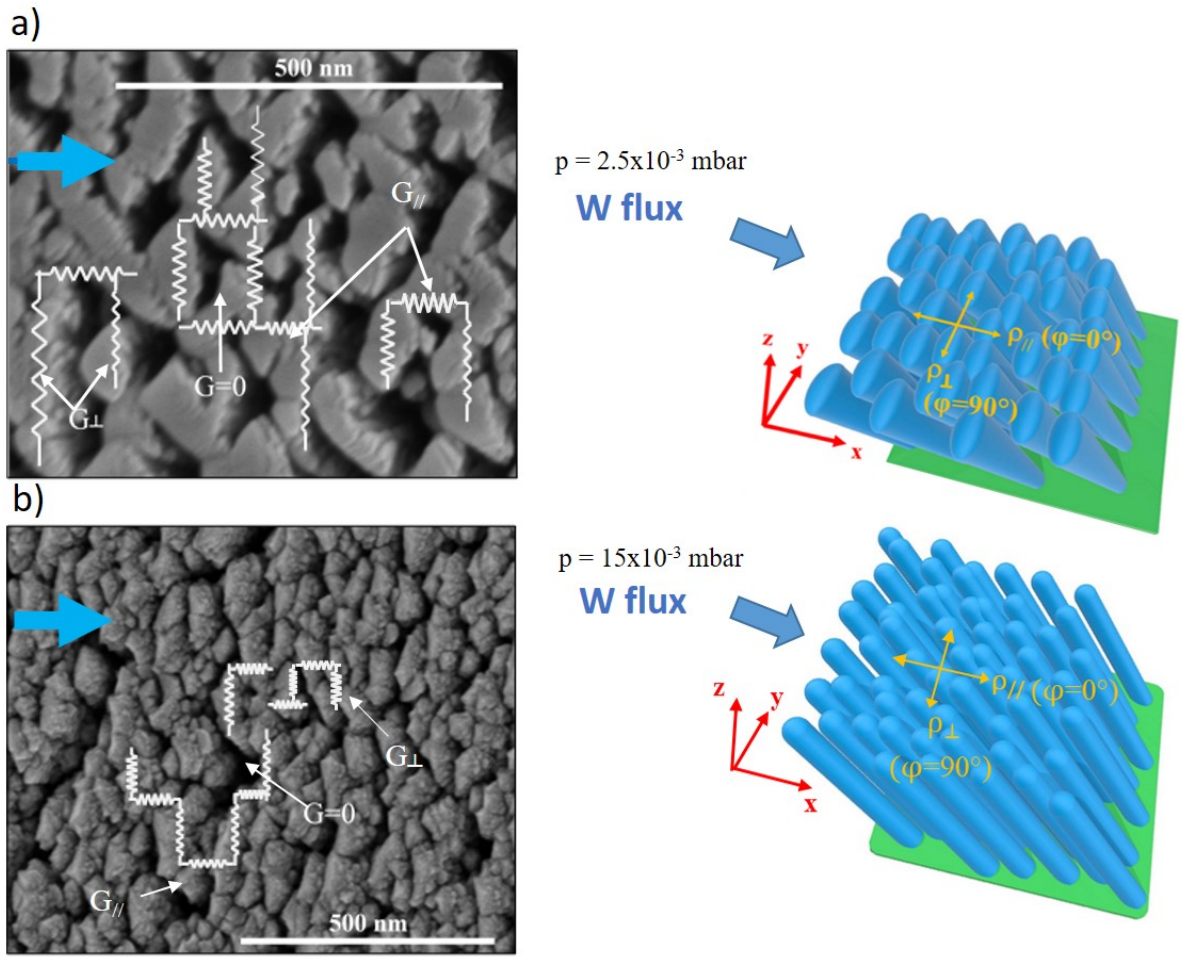

Figure 2: Schematic representation of the variation of conductance directions in the film with SEM observations of two W films 1000 nm thick deposited at: a) 2.5×10^{-3} mbar and b) 15×10^{-3} mbar. Blue arrows indicate the incoming flux of W atoms.

We suppose:

$$G_i = k\sigma\pi\frac{s}{L_{eff}} \quad (1)$$

where σ is the electrical conductivity (Sm^{-1}) of a column (assumed as a bulk material) determined using the Fuchs-Sondheimer theory [34], L_{eff} is the effective conduction length (m) defined as the average length along an individual column that current travels before reaching a node, k is a correction coefficient, and s the cross-sectional area of the columns (m^2) defined by:

$$s = \pi(\frac{d_{eff}}{2})^2 \quad (2)$$

The k value depends on the sputtering pressure used for the deposition. At first, it is assumed that k = 1 at 15×10^{-3} mbar and k = 4 at 2.5×10^{-3} mbar (correlated to the surface area of a column apex). Parameters d_{eff} and L_{eff} are the effective widths of the columns ($d_{//}$ and $d_{\perp}$) and the effective conduction length, respectively. The effective widths are the parallel $d_{//}$ and perpendicular widths $d_{\perp}$ measured from SEM images and presented by a schematic representation in Fig. 3. These widths are considered to be the major parameters influencing the transport of charges (electrons) between columns. The effective parallel width $d_{//}$ is parallel to the particle fluxes. The effective perpendicular width $d_{\perp}$ is perpendicular to the particle fluxes. It decreases with pressure and remains the same after copper etching.

L_{eff} is not directly measurable and has been calculated by the following relation assuming an average value of the film's thickness:

$$L_{eff} = \frac{e_m}{\cos(\beta)} \quad (3)$$

where e_m is the film thickness (nm) and β is the angle of the columns (°).

It is important to note that the contact resistance between the thin columns at the beginning of the growth (as observed in Fig. 3) was neglected. These connections appear during the growth of the nanostructure. Thus, these connections must have minimum resistances, since these individual nanostructures grow together.

4. Results and discussion

4.1. Morphology and structure

4.1.1. W and W-Cu films

Figure 3a shows a cross-section observation of a 1000 nm thick W film sputter-deposited on Si (100) substrate at low pressure (2.5×10^{-3} mbar). A typical tilted columnar structure oriented with an angle of 40±2° can be seen with a distinct fibrous microstructure on top of the columns. Figure 3b is also a cross-section view of W-Cu film with the same thickness (1000 nm), but with a higher column angle of 49±2°.

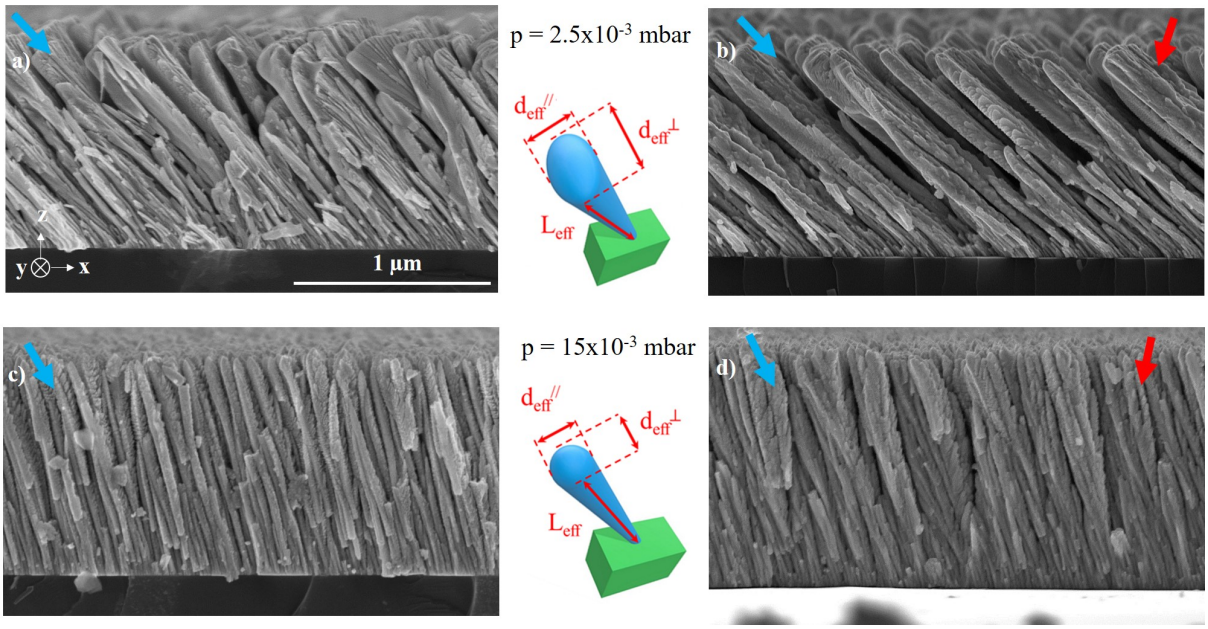

Figure 3: Schematic representation of the variation of effective widths and effective length. Cross-section observations by SEM of W and W-Cu films 1000 nm thick deposited at: a) and c) 2.5×10^{-3} mbar, and b) and d) 15×10^{-3} mbar. Blue and red arrows indicate the direction of incoming W and Cu particle fluxes, respectively.

This higher column angle is due to Cu atoms, which hinder the mobility of W atoms on the top of the columns. This also leads to wider and flatter columns in the direction perpendicular to the W and Cu fluxes. This is also in agreement with the SEM observations of the films

surface (Fig. 4). Wider columns produce a shadowing effect perpendicular to the direction of particle fluxes. These larger columns tend to receive a larger amount of Cu particles. Indeed, for both types of films deposited at low pressure (2.5×10^{-3} mbar), a dense structure is formed at the interface film/substrate whereas during the growth, small columns disappear in favor of larger columns. This phenomenon is specific to the shadowing effect of the GLAD technique [12]. As the thickness increases, the shadowing effect increases and thus more and more spaces develop between the columns. The dense layer at the film/substrate interface is in the order of 100 nm and consists of thin and dense columns. Therefore, growth-stopping columns can be observed for films thicker than or equal to 200 nm. This indicates that competition between columns is permanently present during the film growth.

Figures 3c and d show cross-section views of W and W-Cu films, respectively. Both films were deposited at 15×10^{-3} mbar sputtering pressure and have a thickness of 1000 nm. For these films, the columns are closer to each other compared to those observed for films deposited at 2.5×10^{-3} mbar. They are inclined in the same way and have a relatively constant width throughout the thickness of the film. The column angle of these films is nearly the same, i.e., 15±2º. The dense layer at the substrate/film interface observed for films deposited at 2.5×10^{-3} mbar is not so significant for these W films, but is rather noticed for W-Cu films despite a less inclined architecture. In addition, secondary growths are clearly distinguishable especially on the opposite side of the W target. This is attributed to the W and Cu particle fluxes, which are less directional while increasing the sputtering pressure [35].

The surface observation of W film with a thickness of 1000 nm is shown in figure 4a. This W film is obtained at p = 2.5×10^{-3} mbar and using 140 mA as the current intensity of the W target. This view also shows a heterogeneous surface composed of columns of different width sizes. Thus, wide columns perpendicular to the particle flux are clearly observed. These wide columns have a rough surface composed of fibers. These fibers appear to be thin columns

deposited on a wide column. This form of growth is most visible on the side opposite to the W target [35].

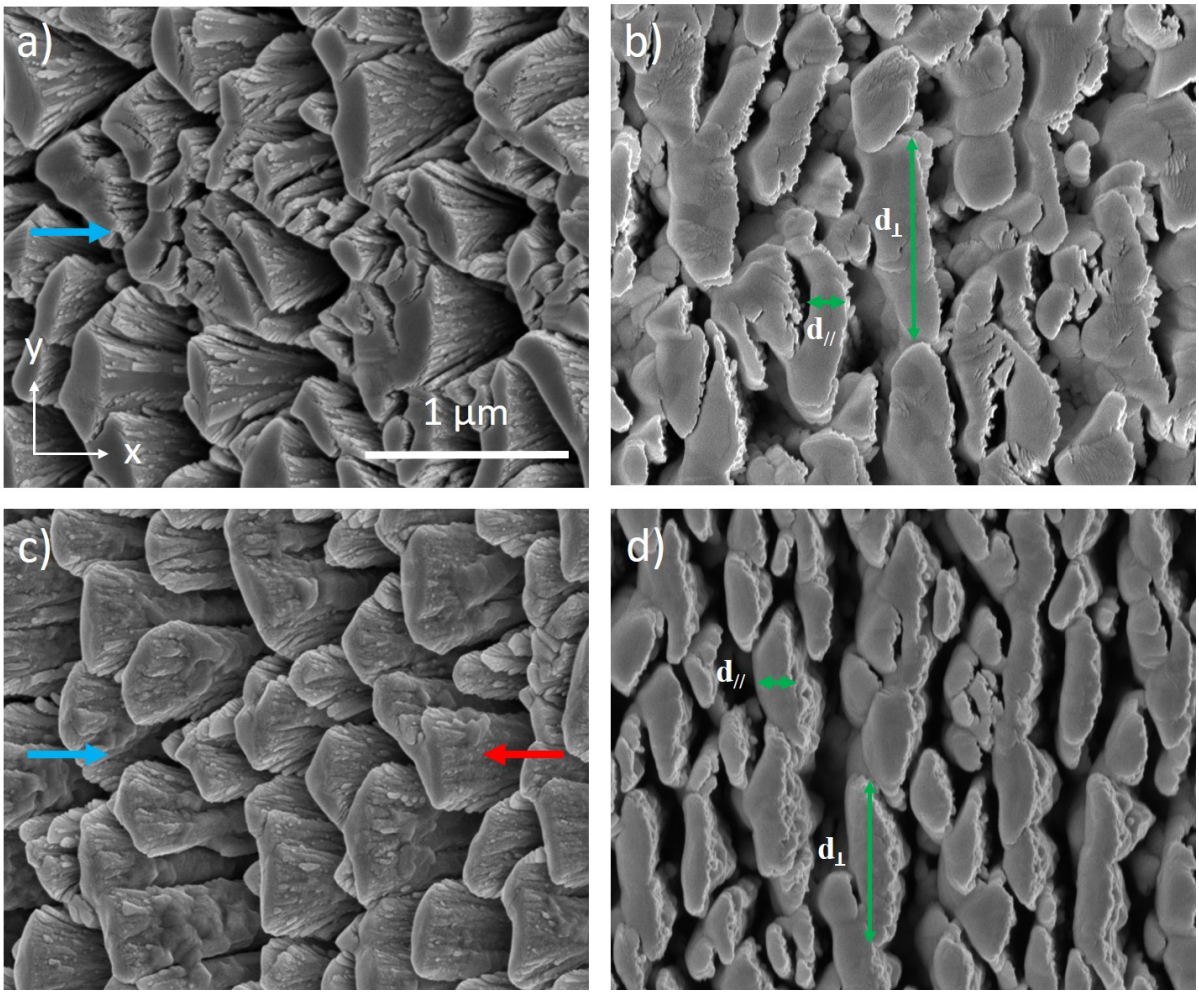

Figure 4: SEM observations of: (a) the surface of W film 1000 nm thick sputter-deposited at 2.5×10^{-3} mbar: (b) the same surface after a tilt of 35°; (c) the surface of a W-Cu film 1000 nm thick; (d) the same surface after a tilt of 45°. Blue and red arrows indicate the direction of incoming W and Cu particle fluxes, respectively.

Figure 4b also shows the surface of this W film and allows the same surface to be observed, but in this case the observation is obtained after tilting the substrate by 35°. This tilt was performed in order to study the structural anisotropy and its influence on the electrical conduction properties. Columns of asymmetrical widths and elliptical shapes can be clearly observed. The dimension $d_\perp$ of the columns along the axis perpendicular to the atomic flux is

systematically larger than that observed parallel $d_{//}$ to the same flux. In addition, the side of the columns facing the flux appears to be smoother than those located at the opposite side (rougher appearance) [35]. The smaller columns tend to stick together to form large columns. As previously explained for W films, the shadowing effect prevails at low pressure. Thus, it leads to a reduced growth on the underside of the column apex, favoring a column widening towards the direction of the deposition source. This is the fanning mechanism [36]. In addition, lateral growth allows neighboring columns to contact each other, while shadowing prevents the merging of columns in the direction parallel to the particle flux. This produces preferential clustering of the column's microstructure in the direction perpendicular to the particle flux. As a result, this fanning mechanism induces an elongated cross-section morphology of the columns.

Image 4c represents the surface of a 1000 nm thick W-Cu film. It was obtained at $p = 2.5\times10^{-3}$ mbar and using 140 mA as the current intensity of the W target and 50 mA as the current intensity of the Cu target. The surface of this film is not homogeneous and is clearly different from that of a pure W film prepared with the same current intensity of W (I_W = 140 mA in figures 4a and b) and with the same thickness. The W side of the W-Cu columns is sharper than the Cu side, which is particularly noticeable on the widest columns. The voids between the columns are more significant than for pure W films. Co-sputtering with W and Cu materials thus gives rise to a different growth mechanism where the flux of Cu atoms disturbs the growth of the W columns. The extinction mechanism [37, 38] of some columns is well observed as a function of the growth. The widening of the columns is clearly visible in figure 4d. The latter shows the surface of W-Cu films by orienting it by -90° towards W and Cu fluxes, and then tilting it by 45° (as for W films deposited at low pressure in figure 4b). This tilting is also very useful to measure more accurately the perpendicular ($d_{\perp}$) and the parallel ($d_{//}$) widths of the columns. It is worth noting that this tilted observation shows how Cu is

deposited on the W columns. Thus, from the side of the W flux, the columns show a steep and smooth profile. From the side of the Cu flux, the columns exhibit a granular and rough profile with Cu grains. In addition, the columns widening is not uniform. The rate of widening differs from one column to another. Incident atoms condense on the apex of the exposed column and contribute to the roughening of the column surface. The roughness of the column apex can become sufficiently important to divide the column into several small columns (secondary growth). This roughness is also an important factor in the fanning rate of the columns. This phenomenon has been reported by Smith *et al.* [36]. The authors studied the growth of the columnar structure and concluded that this increase of the perpendicular width of the columns correspond to the fanning effect. Meakin and Krug [39] studied the evolution of the column tops and described it by the Kardar-Parisi-Zhang (KPZ) model [40]. They showed that the widths $d_{//}$ and $d_{\perp}$ as well as the lengths L of the columns in the x and y directions, respectively, evolve to form columns with elongated cross-sections when the shadowing effect prevails during the growth. Their results corroborate those obtained during the deposition of W-Cu and W films at low pressure (Fig. 4).

Figure 5a shows the surface of W film with a thickness of 1000 nm and deposited at p = 15×10^{-3} mbar.

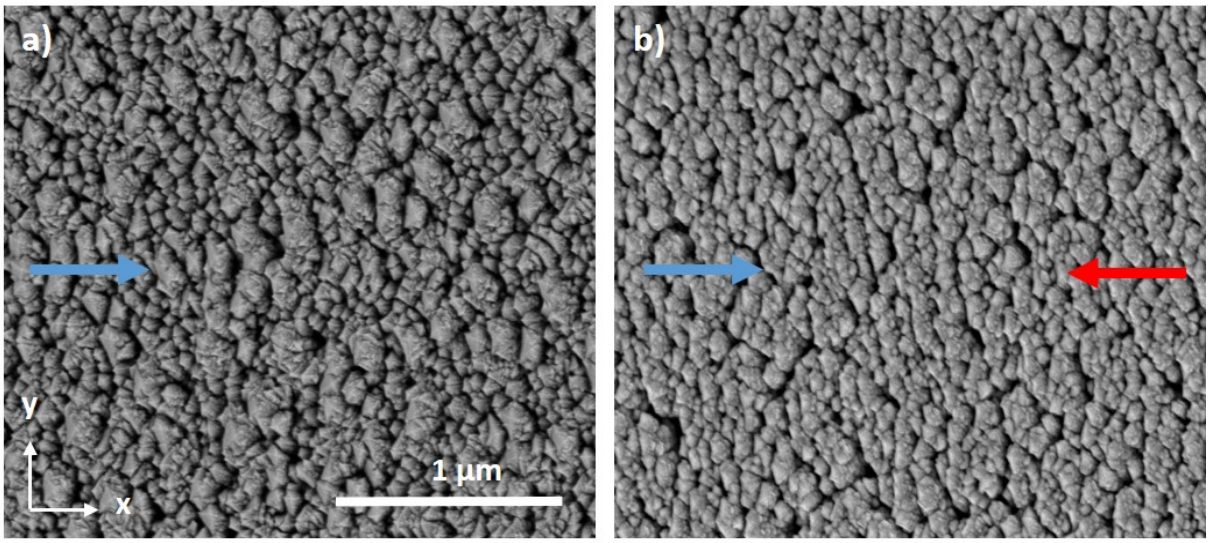

Figure 5: SEM images of: (a) the surface of the W film and (b) the surface of the W-Cu film both deposited at high sputtering pressure (15×10^{-3} mbar) with a thickness of 1000 nm. Blue and red arrows indicate the direction of incoming W and Cu particle fluxes, respectively.

This film exhibits columns with sharp and faceted apexes, which are slightly perpendicular to W flux. The difference of morphology previously observed for W films prepared at low pressure between the columns side facing or opposite to the W flux is not distinguishable. In addition, spaces between the columns are smaller than in the case of films prepared at 2.5×10^{-3} mbar for the same thickness.

Figure 5b shows the surface of W-Cu films deposited at a sputtering pressure of 15×10^{-3} mbar with W and Cu target currents of 140 mA and 50 mA, respectively. The film has a surface composed of columns with similar widths. The columns are grouped together in a circular shape like a bundle (30 to 80 nm according to SEM pictures and values reported in Table 2) of columns with small widths (about 10 nm). It can be seen that there are voids between the columns, but smaller compared to those observed for W-Cu films deposited at 2.5×10^{-3} mbar (Figs. 4a and 4c).

As a result, figure 4 clearly illustrates the anisotropic growth of the columns produced at low pressure whereas a rather isotropic growth is obtained at high pressure, as shown in figure 5. The inclined columnar microstructure exhibits two distinct structural anisotropies. The first relates to the inclination of the column relative to the normal to the substrate and the second corresponds to the development of an elongated perpendicular width of the column. This additional asymmetry results from the shape of the shadow cast on the column by its neighbors at very oblique angles ($\alpha > 80°$).

Figure 6a shows the X-ray diffractograms obtained from W films 1000 nm thick deposited at two different pressures ($p = 2.5\times10^{-3}$ mbar and 15×10^{-3}mbar). Diffraction signals detected at

2θ = 41.58° and 46.76° correspond to the (200) and (210) planes of the body-centered cubic (bcc) β-W phase (ICDD-pdf # 65-6453), respectively. Other diffraction signals detected at 2θ = 47.12° are due to the (110) planes of the bcc α-W phase (ICDD-pdf # 04-0806). On the other hand, both films show a mixture of the β and α-W phases ((200) and (110) peaks). This phase mixture is in agreement with other investigations [41–43] and can be correlated with the change in the microstructural evolution of the films, as already discussed for the SEM images in figures 3, 4 and 5.

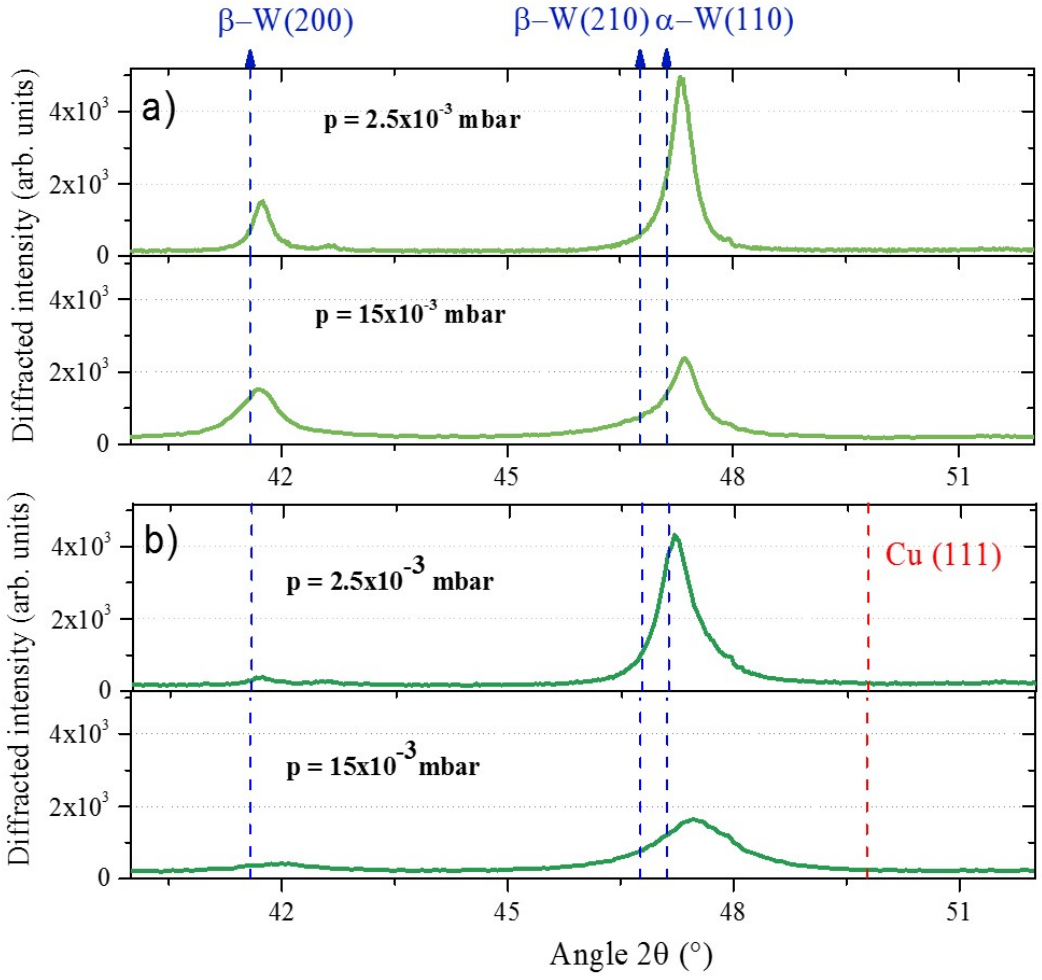

Figure 6: (a) XRD patterns of 1000 nm thick W thin films sputter-deposited on (100) Si substrate with an angle α = 80°, and for an argon sputtering pressure of 2.5×10^{-3} and 15×10^{-3} mbar. (b) XRD patterns of 1000 nm thick W-

Cu thin films sputter-deposited on (100) Si substrate with an angle $\alpha_W = \alpha_{Cu} = 80°$, and for an argon sputtering pressure of 2.5×10^{-3} and 15×10^{-3} mbar.

Since the tilt angle is $\alpha = 80°$, W films deposited at high pressure show intra- and inter-column porosities. Furthermore, the formation of the β-W phase is often accompanied by a porous architecture, some growth defects and a secondary growth [41, 44, 45]. Occurrence of this crystallographic structure is more sensitive to environmental interactions such as residual oxygen, which influences the long-range order and the development of the α-W phase. Indeed, W films deposited at low pressure (2.5×10^{-3} mbar) are better crystallized, since under these conditions, the sputtered particles are energetic and their diffusion on the film surface is favored. At high pressure (15×10^{-3} mbar), W particles become less energetic (thermalization effect), which leads to less organized films and a higher concentration of defects in the columns [46].

X-ray diffractograms recorded for W-Cu films co-deposited at 2.5×10^{-3} and 15×10^{-3} mbar are displayed in figure 6b. These films are produced with $I_W = 140$ mA and $I_{Cu} = 50$ mA with a thickness of 1000 nm. As similarly reported for W films in figure 6a, the diffracted signals correspond to the (110) planes of the bcc α-W phase (ICDD-pdf # 04-0806) and/or $Cu_{0.4}W_{0.6}$ compound (ICDD-pdf #50-1451). These two materials have a very close lattice parameter, which makes difficult the precise determination of the crystallographic phases present in the films. Surprisingly, these films are W-rich and no diffraction signals related to the fcc Cu phase can be noticed, certainly due to the very low crystal size of copper grains (lower than a few nanometers).

Moreover, comparing both diffracted signals located at $2\theta = 47.19°$, the low pressure one is more intense than the high pressure one, due to the improvement of the thermally induced mobility of the W and Cu atoms since during the growth, the film is more exposed to the

directional particle fluxes. As for W films, the high pressure (15.10^{-3} mbar) leads to poorly crystallized W-Cu films. Indeed, Cu atoms disturb the growth of the W lattice, leading to a weakly crystallized metastable solid solution alloy [46]. A high argon sputtering pressure increases the probability of collision between the sputtered W and/or Cu atoms, and argon atoms as they move towards the substrate. As a result, the particle fluxes tend to be less directional and less energetic. As suggested by Vüllers and Spolenak [41], the reduced energy of the incoming W atoms promotes a low mobility adsorption. Other phenomena become negligible, such as the adsorption and implantation of high-mobility atoms prevailing at low sputtering pressure. In addition, migration of W atoms to the growth sites of the α-W phase is hindered and the reduction of W mobility by the adsorbed argon atoms is promoted [47, 48].

It is also interesting noting that the diffracted peaks of these films are systematically shifted towards the higher 2θ angles compared to the theoretical positions. This shift can be attributed to the fact that GLAD films have a high concentration of growth defects such as stacking defects [49] and not to stress [50], this latter decreasing strongly in GLAD films and becoming negligible when the incidence angle of the particle flux is greater than 80°. Aboud *et al.* [51] have shown that the W-Cu system contains deformed tungsten crystallites with a nanometer size. Thus, due to the immiscibility of the W and Cu metals, and assuming that the films are prepared from a co-sputtering process, some solid solutions may be obtained at the W/Cu interfaces inside a column.

4.1.2. Chemical etching of W-Cu films

Since the electrical properties of thin films can be tuned by means of their porosity, a wet chemical etching was therefore carried out to remove the copper from the W-Cu films. Morphology and structure of these films were characterized before and after copper etching. SEM analyses were performed before and after copper etching and are presented in figure 7.

The films surface was observed without inclination and then afterwards with a 35° inclination at the same location. The view of the surface without inclination (Fig. 7a) and before Cu etching, clearly shows fibers and grains on the top of the columns, as well as a steep profile in front of the W flux side. Grains appear darker than fibers, and are observed on the opposite side (i.e., facing the Cu flux). After Cu etching, the fibrous structure is better distinguished and the granular aspect previously noticed on the side of the columns facing the Cu flux, becomes less defined.

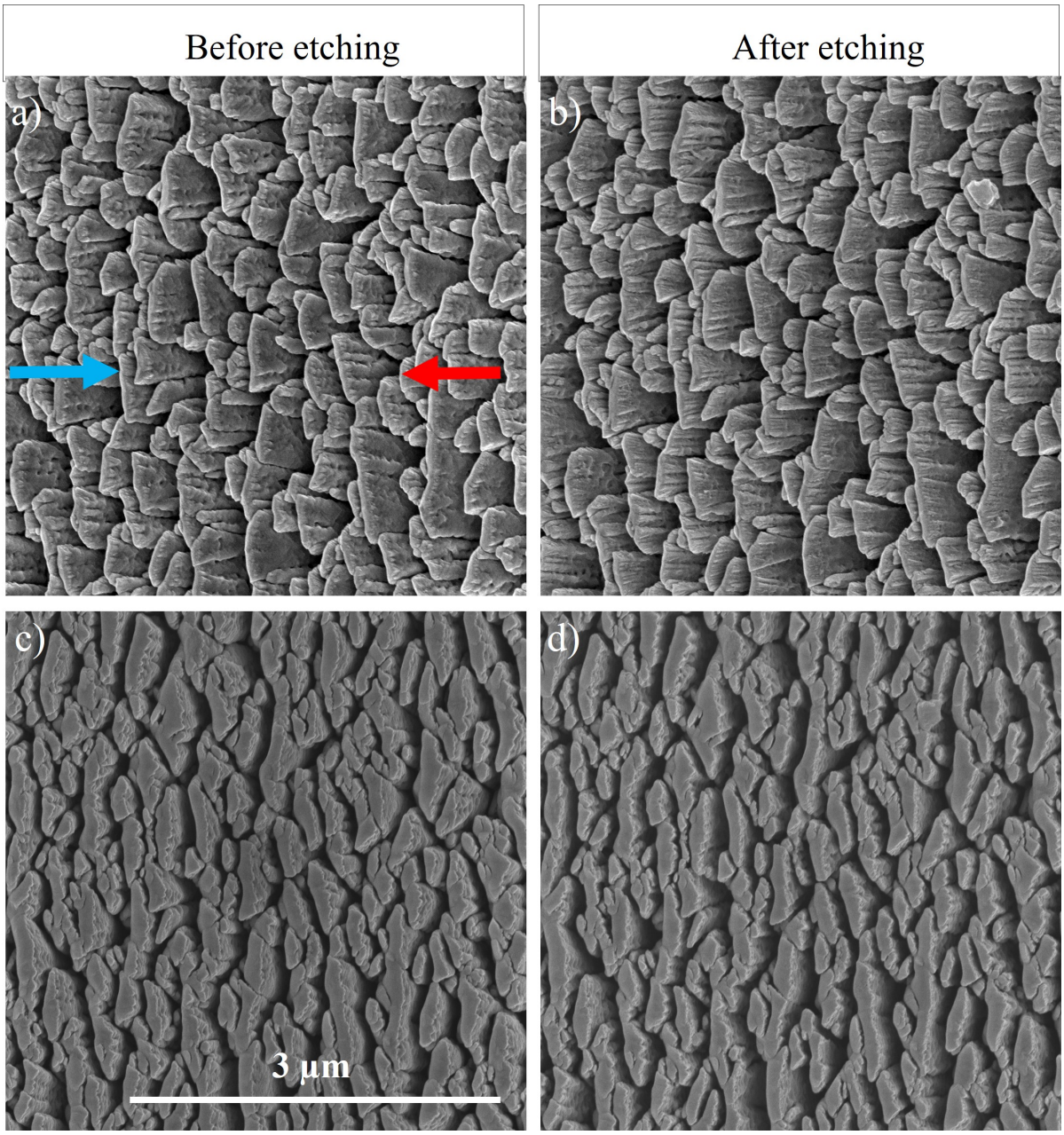

Figure 7: SEM images of the surface of a W-Cu film 1000 nm thick viewed at the same location: a) before and b) after Cu etching, and with a 45° tilt angle of observation: c) before and d) after Cu etching. Blue and red arrows indicate the direction of incoming W and Cu particle fluxes, respectively.

It is interesting to note that columns in W-Cu etched films are more spaced in the direction perpendicular to the W and Cu fluxes. In addition, figure 7 shows the surface view after tilting the sample of 35°, before (Fig. 7c) and after Cu etching (Fig. 7d). This observation allows us to verify that the shape of the columns remains the same, but with a narrower width. From these images, the columns rather show a serrated shape on Cu flux side, whereas the abrupt profile is kept on W flux side.

The parallel width ($d_{//}$) before Cu etching is larger than after, while for the perpendicular width ($d_{\perp}$) it remains the same. This result supports that a certain amount of copper has been removed and confirms that the deposition mainly occurs in the direction perpendicular to the particle flux. However, one cannot state that all the copper is completely etched, since former investigations show that about 12 at. % of copper remains in W-Cu films after this chemical etching procedure [3]. The observed structure may correspond to the grains of the $Cu_{0.4}W_{0.6}$ compound, which has a lattice constant very close to the α-W phase detected from X-ray diffraction analyses (XRD patterns of W-Cu etched films similar to the pattern in Fig. 6b).

4.2. Electrical properties

4.2.1. From measurements

In order to study the anisotropy of the electrical resistivity as a function of the azimuthal angle of the columns, measurements of the electrical resistivity were performed using the Bierwagen's method, as previously described in § 3. These measurements were carried out at room temperature on W and W-Cu films before and after copper etching. The films studied have the same thickness of 1000 nm and are deposited at two different pressures: 2.5×10^{-3} and

15×10^{-3} mbar. These samples were rotated at different azimuthal angles φ ranging from 0° to 180°. At each angle step, the electrical resistivity was measured in the direction of the angle (Fig. 1). For all films, the variation of the electrical resistivity as a function of the azimuthal angle is shown in figure 8.

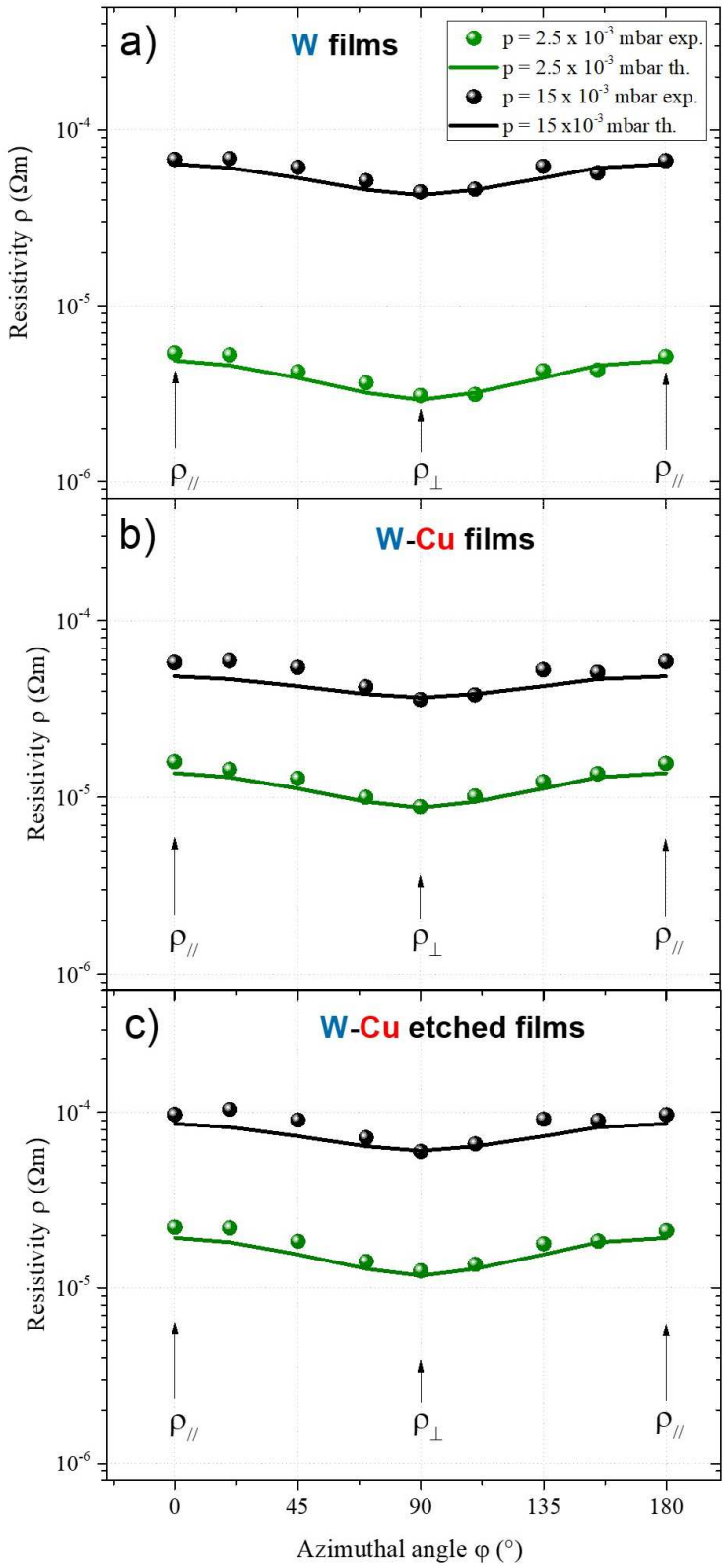

Figure 8: Variation of electrical resistivity measured at room temperature (300 K) as a function of azimuthal angle φ for: a) W films, b) W-Cu films and c) etched W-Cu films 1000 nm thick sputter-deposited at 2.5×10^{-3} and 15×10^{-3} mbar. $\rho_{//}$ et $\rho_{\perp}$ represent resistivity in the direction parallel and perpendicular to W and Cu fluxes,

respectively. Symbols correspond to experimental resistivity (exp.) and solid lines correspond to theoretical resistivity (th.).

The highest resistivity anisotropy well correlates with the microstructural anisotropy clearly shown by SEM pictures for the films deposited at low pressure (Figs. 4a and 4b). For such deposition conditions, columns with elongated cross-section in the direction perpendicular to the W flux have been brought to the fore. With a large increase of the sputtering pressure (i.e., at 15×10^{-3} mbar), this resistivity anisotropy slightly diminishes but still remains significant despite more bundled and homogeneous columns shape with less anisotropic cross-sections.

Figure 8b shows the electrical resistivity measurements of W-Cu films before copper etching. For W-Cu films prepared at 15×10^{-3} mbar, $\rho_{//} = 5.81\times10^{-5}$ Ωm and $\rho_{\perp}= 3.58\times10^{-5}$ Ωm, which corresponds to an anisotropic coefficient A = 1.62. Such values are close to those measured for W films produced at this high sputtering pressure. These results are also in agreement with the very similar surface morphology viewed by SEM in figure 5 (bundling effect of the columns due to a less directional particle flux at high pressure). Lowering the sputtering pressure down to 2.5×10^{-3} mbar does not lead to a substantial drop of W-Cu films resistivity (compared to W films) since $\rho_{//} = 1.59\times10^{-5}$ Ωm and $\rho_{\perp}= 8.83\times10^{-6}$ Ωm, but the anisotropic coefficient remains important and similar to that of W films with A = 1.80. Such a relevant anisotropy correlates with the elongated cross-sections of W-Cu columns clearly noticed from SEM observations (Figs. 4a and 7c). In addition, one could expect more resistive W-Cu films as the microstructure exhibits more bundled columns well separated by voids than that of W films (Fig. 4b). However, the large content of Cu in the films (W-to-Cu atomic concentration ratio is about 3 [27]) enhances the overall conductivity of W-Cu films.

After Cu etching, W-Cu films become more resistive for both sputtering pressures (Fig. 8c). This trend to become more resistive is assigned to the more voided architecture induced by

the partially removal of Cu in the films (Cu trapped in the first growing stage of the W-Cu films cannot be completely etched due to the dense structure obtained for the first few tens nanometers of thickness). On the other hand, the Cu concentration significantly drops from 23±5 at. % to 12±5 at. % whatever the sputtering pressure before after and after chemical etching, respectively. This loss of Cu also contributes to increase the films' resistivity. In addition, the anisotropy coefficient is close to 1.6 at high pressure. This coefficient reaches 1.91 for films prepared at 2.5×10^{-3} mbar, which is the highest anisotropic resistivity produced after W-Cu etching. It agrees with SEM images in figure 7. Without rotation and tilting of the sample (Fig. 7a and b), the fibrous morphology of the columns side locate in front of the Cu flux is better defined after Cu etching. The granular aspect of Cu grains grown on W columns is weakened since a part of unalloyed copper was chemically removed from the films. Voids between columns are broadened and the tilted columnar architecture is kept, which is imposed by the anisotropic growth of W (Fig. 7d). Resistivity of W-Cu films sputter-deposited at 15×10^{-3} mbar is even more sensitive to the chemical etching since the less directional flux of sputtered particles induced by the sputtering pressure acts as a spreading effect on the columnar structure. Copper atoms are more distributed around the W columns and the etching is more efficient.

4.2.2. From calculation

By injecting the resistivity calculated according to the AB^2-EMA theory into a rotation tensor, one can plot the evolution of the resistivity calculated as a function of the azimuthal angle. For all the films, the resistivity obtained with the AB^2-EMA theory shows a relatively good matching with the experimental values (solid lines in Fig. 8). It is important noting that in order to find the best correlation between the calculated and measured resistivity values, perpendicular and parallel widths of the columns ($d_\perp$ and $d_{//}$, respectively) were adjusted.

Table 2 shows experimental and calculated $d_{\perp}$ and $d_{//}$ values obtained for W, W-Cu and W-Cu etched films (experimental values and associated standard errors are calculated from the weighted arithmetic mean of the column widths distribution obtained from SEM pictures with a tilt viewing).

	2.5×10^{-3} mbar				15×10^{-3} mbar			
	Experiment (nm)		Calculated (nm)		Experiment (nm)		Calculated (nm)	
	//	⊥	//	⊥	//	⊥	//	⊥
W	158±67	500±180	125	571	40±17	79±31	28	120
W-Cu	144±42	350±140	100	450	35±15	68±27	20	102
Etched W-Cu	133±39	350±140	88	420	34±15	67±27	30	131

Table 2: Calculated and experimental values of perpendicular and parallel widths ($d_{//}$ and $d_{\perp}$, respectively) of columns in W, W-Cu and etched W-Cu films sputter-deposited at 2.5×10^{-3} and 15×10^{-3} mbar.

As previously observed from SEM pictures (Figs. 2, 4, 5 and 7), a difference is systematically obtained between the $d_{\perp}$ and $d_{//}$ experimental values, whatever the sputtering pressure and the type of films. For all films deposited at high pressure, both experimental widths reduce especially $d_{\perp}$, which is lower than 80 nm. However, $d_{\perp}$ remains about twice higher than $d_{//}$. This means that a structural anisotropy carries on despite more dispersive W and Cu particle fluxes induced by the high sputtering pressure. Theoretical $d_{//}$ and $d_{\perp}$ values adjusted from the model follow the same trend, i.e., smaller widths as the pressure rises and $d_{\perp}$ is always higher than $d_{//}$. In addition, it is worth noting that for all films produced with the lowest sputtering pressure, the model corroborates the strong anisotropic columnar cross-section with $d_{\perp}$

theoretical values, which are three to four times higher than those obtained for parallel widths $d_{//}$.

For the high pressure, $d_{//}$ and $d_{\perp}$ theoretical widths exhibit more discrepancy towards experimental values. This difference can be assigned to a higher concentration of structural defects. By increasing the sputtering pressure up to 15×10^{-3} mbar, sputtered atoms impinge on the growing film with an energy below 1 eV [52]. As a result, they arrive on the apex of the columns with a large dispersion and with a low surface mobility. It disturbs the long-range order of grains inside the tilted columns and thus favors growing and surface defects such as atomic vacancies and deficiencies. These defects are neglected in the model leading to more divergence between theoretical and experimental columns widths adjusted at high pressure.

Basically, the used model validates experimental measurements and supports that the resistivity of the films decreases with the length of the columns as well as with the increase of the perpendicular width of the columnar cross-section. These transport properties are related to the increasing connectivity of the perpendicular width of the columns, which promotes conduction paths for the charge carriers (electrons in our films). These results establish that the AB^2-EMA analytical model can be successfully implemented to describe the electrical conductivity of GLAD films formed of columnar architectures. Such a model provides a useful tool for structural characterization. It also explains the influence of the column geometry on the electrical resistivity of GLAD films. Last but not least, it is interesting to note that the dense layer/substrate interface is not assumed in the model. The use of percolation theory makes it possible to establish a relationship between morphological parameters and microstructure, which can lead to the determination of other physical properties of structured thin films.

5. Conclusion

W and W-Cu thin films were prepared by GLAD sputtering and co-sputtering using two argon sputtering pressures: 2.5×10^{-3} and 15×10^{-3} mbar. The effect of these extreme pressures on the structure, morphology and electrical resistivity of these films was studied. A low sputtering pressure (2.5×10^{-3} mbar) favors the directionality of atoms impinging on the growing films. A ballistic character of the sputtered particles prevails and leads to a tilted columnar structure with a strong anisotropic structure of the column cross-section, perpendicular to the particle fluxes. Such a dominant lateral growth produces a better electronic transport and thus, a strong resistivity anisotropy. The latter is enhanced by means of a wet chemical etching of copper in W-Cu thin films. Depositing at high sputtering pressure (15×10^{-3} mbar) gives rise to more dispersion of the sputtering flux. The elongated columnar cross-section of the films obtained at low pressure nearly vanishes, although the resistivity anisotropy still remains significant.

In order to better understand the role of columns geometry on electrical properties of these films, the effective medium method was used to model the resistivity anisotropy of W and W-Cu films. It was shown that the experimental results are well described by the AB^2-EMA model. Anisotropic behaviors of resistivity can be accurately estimated, especially by adjusting the size of the column cross-sections. For the films prepared at low sputtering pressure, the used model well agrees with large column widths in the direction perpendicular to the particle fluxes and so, with the highest resistivity anisotropy. Operating at high sputtering pressure, resistivity anisotropy is kept but becomes less substantial. Modelling confirms the reduction of the columns' width following the parallel direction ($d_{//}$) of the particle fluxes.

Finally, electronic transport properties in metallic GLAD thin films prepared by sputtering and co-sputtering can be clearly related to the increasing connectivity between columns,

which is enhanced or reduced as a function of the columnar cross-section morphology. Results presented in this article well establish that the effective medium used in this percolation model is a valuable tool to precisely describe the conductivity of columns arrays and provide a useful insight into structural characteristics of tilted columnar thin films. Implementing such a model allows the determination of relevant relationships between some morphological parameters of the films, their microstructure, and the growing conditions.

CRediT authorship contribution statement

Raya El Beainou: Data curation, Formal analysis, Writing – original draft. **Jean-Marc Cote:** Software, Data curation, Investigation. **Vincent Tissot:** Resources, Data curation, Methodology. **Valérie Potin:** Writing - review & editing, Supervision, Funding acquisition. **Nicolas Martin:** Writing - review & editing, Supervision, Funding acquisition

Declaration of Competing Interest

The authors declare that they have no known competing financial interests or personal relationships that could have appeared to influence the work reported in this paper.

Acknowledgements

This work was supported by the EIPHI Graduate School (contract ANR-17-EURE-0002), the Region of Franche-Comté and the French RENATECH network.

References

[1] K.D. Harris, D. Vick, M.J. Brett, K. Robbie, Improved microstructures for thermal barrier coatings produced by Glancing Angle Deposition, MRS Proc. 555 (1998) 97. https://doi.org/10.1557/PROC-555-97.

[2] B. Mohanty, B.D. Morton, A. Sinan Alagoz, T. Karabacak, M. Zou, Frictional anisotropy of tilted molybdenum nanorods fabricated by glancing angle deposition, Tribol. Int. 80 (2014) 216–221. https://doi.org/10.1016/j.triboint.2014.07.010.

[3] R. El Beainou, R. Salut, L. Robert, J.-M. Cote, V. Potin, N. Martin, Anisotropic conductivity enhancement in inclined W-Cu columnar films, Mater. Lett. 232 (2018) 126–129. https://doi.org/10.1016/j.matlet.2018.08.120.

[4] N. Martin, J. Sauget, T. Nyberg, Anisotropic electrical resistivity during annealing of oriented columnar titanium films, Mater. Lett. 105 (2013) 20–23. https://doi.org/10.1016/j.matlet.2013.04.058.

[5] C. Song, G.K. Larsen, Y. Zhao, Anisotropic resistivity of tilted silver nanorod arrays: Experiments and modeling, Appl. Phys. Lett. 102 (2013) 233101. https://doi.org/10.1063/1.4809951.

[6] E. Coffy, G. Dodane, S. Euphrasie, A. Mosset, P. Vairac, N. Martin, H. Baida, J.M. Rampnoux, S. Dilhaire, Anisotropic propagation imaging of elastic waves in oriented columnar thin films, J. Phys. Appl. Phys. 50 (2017) 484005. https://doi.org/10.1088/1361-6463/aa92ad.

[7] R. El Beainou, A. Chargui, P. Pedrosa, A. Mosset, S. Euphrasie, P. Vairac, N. Martin, Electrical resistivity and elastic wave propagation anisotropy in glancing angle deposited tungsten and gold thin films, Appl. Surf. Sci. 475 (2019) 606–614. https://doi.org/10.1016/j.apsusc.2019.01.041.

[8] A. Chargui, R. El Beainou, A. Mosset, S. Euphrasie, V. Potin, P. Vairac, N. Martin, Influence of thickness and sputtering pressure on electrical resistivity and elastic wave propagation in oriented columnar tungsten thin films, Nanomaterials. 10 (2020) 81. https://doi.org/10.3390/nano10010081.

[9] M. Mansour, A.-S. Keita, B. Gallas, J. Rivory, A. Besnard, N. Martin, Optical anisotropy of tilted columns thin films of chromium deposited at oblique incidence, Opt. Mater. 32 (2010) 1146–1153. https://doi.org/10.1016/j.optmat.2010.03.022.

[10] S. Keitoku, K. Nishioka, Grain structure and magnetic anisotropy of Fe film evaporated obliquely from two sources, Jpn. J. Appl. Phys. 20 (1981) 1249–1253. https://doi.org/10.1143/JJAP.20.1249.

[11] K. Robbie, M.J. Brett, Sculptured thin films and glancing angle deposition: Growth mechanics and applications, J. Vac. Sci. Technol. Vac. Surf. Films. 15 (1997) 1460–1465. https://doi.org/10.1116/1.580562.

[12] M.M. Hawkeye, M.T. Taschuk, M.J. Brett, Glancing angle deposition of thin films: Engineering the nanoscale, John Wiley & Sons, Ltd, Chichester, UK, 2014.

[13] A. Barranco, A. Borras, A.R. Gonzalez-Elipe, A. Palmero, Perspectives on oblique angle deposition of thin films: From fundamentals to devices, Prog. Mater. Sci. 76 (2016) 59–153. https://doi.org/10.1016/j.pmatsci.2015.06.003.

[14] C. Charles, N. Martin, M. Devel, J. Ollitrault, A. Billard, Correlation between structural and optical properties of WO_3 thin films sputter deposited by glancing angle deposition, Thin Solid Films. 534 (2013) 275–281. https://doi.org/10.1016/j.tsf.2013.03.004.

[15] M.M. Hawkeye, R. Joseph, J.C. Sit, M.J. Brett, Coupled defects in one-dimensional photonic crystal films fabricated with glancing angle deposition, Opt. Express. 18 (2010) 13220. https://doi.org/10.1364/OE.18.013220.

[16] Y. Ueda, W. Takakura, A. Yamada, Electrical resistivity and magnetism of Fe/Si multilayers prepared by oblique incidence evaporation, J. Magn. Magn. Mater. 239 (2002) 45–47. https://doi.org/10.1016/S0304-8853(01)00616-3.

[17] H. Du, H. Chen, J. Gong, T.G. Wang, C. Sun, S.W. Lee, L.S. Wen, Use of effective medium theory to model the effect of the microstructure on dc conductivity of nano-titanium films, Appl. Surf. Sci. 233 (2004) 99–104. https://doi.org/10.1016/j.apsusc.2004.03.214.

[18] J.R. Sambles, The resistivity of thin metal films—Some critical remarks, Thin Solid Films. 106 (1983) 321–331. https://doi.org/10.1016/0040-6090(83)90344-9.

[19] G. Baccarani, B. Riccò, G. Spadini, Transport properties of polycrystalline silicon films, J. Appl. Phys. 49 (1978) 5565–5570. https://doi.org/10.1063/1.324477.

[20] D.K. Pandya, A.C. Rastogi, K.L. Chopra, Obliquely deposited amorphous Ge films. I. Growth and structure, J. Appl. Phys. 46 (1975) 2966–2975. https://doi.org/10.1063/1.321984.

[21] M.M. Steeves, D. Deniz, R.J. Lad, Charge transport in flat and nanorod structured ruthenium thin films, Appl. Phys. Lett. 96 (2010) 142103. https://doi.org/10.1063/1.3377006.

[22] Y. Zhong, Y.C. Shin, C.M. Kim, B.G. Lee, E.H. Kim, Y.J. Park, K.M.A. Sobahan, C.K. Hwangbo, Y.P. Lee, T.G. Kim, Optical and electrical properties of indium tin oxide thin films with tilted and spiral microstructures prepared by oblique angle deposition, J. Mater. Res. 23 (2008) 2500–2505. https://doi.org/10.1557/jmr.2008.0312.

[23] D. Vick, M.J. Brett, Conduction anisotropy in porous thin films with chevron microstructures, J. Vac. Sci. Technol. Vac. Surf. Films. 24 (2006) 156–164. https://doi.org/10.1116/1.2148413.

[24] A. Besnard, N. Martin, L. Carpentier, B. Gallas, A theoretical model for the electrical properties of chromium thin films sputter deposited at oblique incidence, J. Phys. Appl. Phys. 44 (2011) 215301. https://doi.org/10.1088/0022-3727/44/21/215301.

[25] C.R. Pichard, C.R. Tellier, A.J. Tosser, A three-dimensional model for grain boundary resistivity in metal films, Thin Solid Films. 62 (1979) 189–194. https://doi.org/10.1016/0040-6090(79)90305-5.

[26] S. Kirkpatrick, Percolation and Conduction, Rev. Mod. Phys. 45 (1973) 574–588. https://doi.org/10.1103/RevModPhys.45.574.

[27] R. El Beainou, N. Martin, V. Potin, P. Pedrosa, M.A.P. Yazdi, A. Billard, Correlation between structure and electrical resistivity of W-Cu thin films prepared by GLAD co-sputtering, Surf. Coat. Technol. 313 (2017) 1–7. https://doi.org/10.1016/j.surfcoat.2017.01.039.

[28] R. El Beainou, N. Martin, V. Potin, P. Pedrosa, M.A.P. Yazdi, A. Billard, W-Cu sputtered thin films grown at oblique angles from two sources: Pressure and shielding effects, Surf. Coat. Technol. 343 (2018) 153–159. https://doi.org/10.1016/j.surfcoat.2017.09.062.

[29] S. Mahieu, P. Ghekiere, D. Depla, R. De Gryse, Biaxial alignment in sputter-deposited thin films, Thin Solid Films, 515 (2006) 1229-1249. https://doi.org/10.1016/j.tsf.2006.06.027.

[30] G. Abadias, F. Angay, R. Mareus, C. Mastail, Texture and stress evolution in HfN films sputter-deposited at oblique angles, Coatings, 9 (2019) 712-15. https://doi.org/10.3390/coatings9110712.

[31] L.J. van der Pauw, A method of measuring specific resistivity and Hall effect of discs of arbitrary shape, Philips Res Rep. 13 (1958) 1–9. https://doi.org/10.1142/9789814503464_0017.

[32] O. Bierwagen, R. Pomraenke, S. Eilers, W.T. Masselink, Mobility and carrier density in materials with anisotropic conductivity revealed by van der Pauw measurements, Phys. Rev. B. 70 (2004) 165307. https://doi.org/10.1103/PhysRevB.70.165307.

[33] J. Bernasconi, Conduction in anisotropic disordered systems: Effective-medium theory, Phys. Rev. B. 9 (1974) 4575–4579. https://doi.org/10.1103/PhysRevB.9.4575.

[34] R. G. Chambers, The conductivity of thin wires in a magnetic field, Proc. R. Soc. Lond. Ser. Math. Phys. Sci. 202 (1950) 378–394. https://doi.org/10.1098/rspa.1950.0107.

[35] R. El Beainou, A. Garcia-Valenzuela, M. Raschetti, J.-M. Cote, R. Alvarez, A. Palmero, V. Potin, N. Martin, A 4-view imaging to reveal microstructural differences in obliquely sputter-deposited tungsten films, Mater. Lett. 264 (2020) 127381. https://doi.org/10.1016/j.matlet.2020.127381.

[36] D.O. Smith, M.S. Cohen, G.P. Weiss, Oblique-incidence anisotropy in evaporated permalloy films, J. Appl. Phys. 31 (1960) 1755–1762. https://doi.org/10.1063/1.1735441.

[37] S. Mukherjee, D. Gall, Anomalous scaling during glancing angle deposition, Appl. Phys. Lett. 95 (2009) 173106. https://doi.org/10.1063/1.3257377.

[38] S. Mukherjee, D. Gall, Power law scaling during physical vapor deposition under extreme shadowing conditions, J. Appl. Phys. 107 (2010) 084301. https://doi.org/10.1063/1.3385389.

[39] P. Meakin, J. Krug, Columnar microstructure in three-dimensional ballistic deposition, Europhys. Lett. EPL. 11 (1990) 7–12. https://doi.org/10.1209/0295-5075/11/1/002.

[40] M. Kardar, G. Parisi, Y.-C. Zhang, Dynamic scaling of growing interfaces, Phys. Rev. Lett. 56 (1986) 889–892. https://doi.org/10.1103/PhysRevLett.56.889.

[41] F.T.N. Vüllers, R. Spolenak, Alpha- vs. beta-W nanocrystalline thin films: A comprehensive study of sputter parameters and resulting materials' properties, Thin Solid Films. 577 (2015) 26–34. https://doi.org/10.1016/j.tsf.2015.01.030.

[42] K. Salamon, O. Milat, N. Radić, P. Dubček, M. Jerčinović, S. Bernstorff, Structure and morphology of magnetron sputtered W films studied by x-ray methods, J. Phys. Appl. Phys. 46 (2013) 095304. https://doi.org/10.1088/0022-3727/46/9/095304.

[43] K.R. Khedir, G.K. Kannarpady, H. Ishihara, J. Woo, C. Ryerson, A.S. Biris, Morphology control of tungsten nanorods grown by glancing angle RF magnetron sputtering under variable argon pressure and flow rate, Phys. Lett. A. 374 (2010) 4430–4437. https://doi.org/10.1016/j.physleta.2010.08.066.

[44] D. Choi, B. Wang, S. Chung, X. Liu, A. Darbal, A. Wise, N.T. Nuhfer, K. Barmak, A.P. Warren, K.R. Coffey, M.F. Toney, Phase, grain structure, stress, and resistivity of sputter-deposited tungsten films, J. Vac. Sci. Technol. Vac. Surf. Films. 29 (2011) 051512. https://doi.org/10.1116/1.3622619.

[45] M.J. O'Keefe, J.T. Grant, Phase transformation of sputter deposited tungsten thin films with A-15 structure, J. Appl. Phys. 79 (1996) 9134–9141. https://doi.org/10.1063/1.362584.

[46] C.-S. Xiong, Y.-H. Xiong, H. Zhu, T.-F. Sun, E. Dong, G.-X. Liu, Synthesis and structural studies of the Cu-W alloys prepared by mechanical alloying, Nanostructured Mater. 5 (1995) 425–432. https://doi.org/10.1016/0965-9773(95)00252-A.

[47] Y.G. Shen, Y.W. Mai, Q.C. Zhang, D.R. McKenzie, W.D. McFall, W.E. McBride, Residual stress, microstructure, and structure of tungsten thin films deposited by magnetron sputtering, J. Appl. Phys. 87 (2000) 177–187. https://doi.org/10.1063/1.371841.

[48] J.A. Thornton, Influence of apparatus geometry and deposition conditions on the structure and topography of thick sputtered coatings, J. Vac. Sci. Technol. 11 (1974) 666–670. https://doi.org/10.1116/1.1312732.

[49] S. Tamulevičius, Stress and strain in the vacuum deposited thin films, Vacuum 51 (1998) 127–139. https://doi.org/10.1016/S0042-207X(98)00145-6.

[50] T. Karabacak, C.R. Picu, Jay.J. Senkevich, G.-C. Wang, T.-M. Lu, Stress reduction in tungsten films using nanostructured compliant layers, J. Appl. Phys. 96 (2004) 5740–5746. https://doi.org/10.1063/1.1803106.

[51] T. Aboud, B.-Z. Weiss, R. Chaim, Mechanical alloying of the immiscible system W-Cu, Nanostructured Mater. 6 (1995) 405–408. https://doi.org/10.1016/0965-9773(95)00082-8.

[52] R.E. Somekh, Calculations of thermalization during the sputter deposition process, Vacuum, 34(10-11) (1984), 987-990. https://doi.org/10.1016/0042-207X(84)90183-0.

Anisotropic W and W-Cu films

$\rho_x > \rho_y$